P6.4 SIMULATIONS VERSUS OBSERVATIONS OF A SHEARED CONVECTIVE BOUNDARY LAYER

Robert J. Conzemius*
WindLogics, Inc.
Grand Rapids, Minnesota, USA

Evgeni Fedorovich
School of Meteorology, University of Oklahoma
Norman, Oklahoma, USA

I. INTRODUCTION

Large eddy simulation (LES) is a numerical technique that is highly suitable to the study of idealized flows, particularly the atmospheric convective boundary layer (CBL). However, for the study of particular cases, where the flow is driven by larger scale forcing, the application of this technique is a bit more challenging since present day computer power does not allow the simulation of all relevant scales of atmospheric motion. Two approaches that confront this problem are the use of multiple nested grids within a numerical weather prediction model (Moeng et al. 2007) and simply representing the forcing from atmospheric processes larger than the LES domain scale by using additional terms in the LES equations (Conzemius 2004). The present study focuses on the latter.

The case for this particular study was a CBL during the 22 MAY 2002 observations taken as a part of the International H2O Project (IHOP_2002) experiment (Weckwerth et al. 2004)—a day in which the wind shear was relatively strong and was a significant contributor to the CBL dynamics (Conzemius and Fedorovich 2006). A vast dataset of observations was available from the IHOP_2002 experiment for this particular case, which presented some of the best conditions during IHOP_2002 for comparing the observed evolution of the sheared atmospheric CBL with LES (Moeng and Sullivan 1994; Pino et al. 2003; Conzemius and Fedorovich 2006).

The primary goals of the study are threefold. First, we intend to evaluate LES predictions of the sheared CBL evolution against lidar observations of CBL depth evolution and to additionally compare LES output with radiometer, radar, and radiosonde data to more fully understand the evolution of the mean wind and temperature in the CBL. The second major goal of the presented study is to compare the growth of the simulated CBL with that of the observed CBL to understand the relative importance of various factors that determine the CBL growth for this case. Some of these, such as entrainment dynamics, might be well simulated, but others, such as large scale atmospheric vertical motion, might not. Despite its limitations, LES shows promise for simulating real cases, and it will likely have important applications in the future (in particular, to the wind energy industry) because of its ability to resolve nonsteady, turbulent flows. Thus, identifying successes and drawbacks of LES for actual atmospheric cases is essential for its application. Finally, we seek to compare the turbulence structures of LES with those observed on 22 MAY 2002.

Fig. 1. Locations of LES grid and observational data input to LES. Large squares indicate the position of NWS radiosonde observations, triangles denote the locations of ISFF sites, and the S-Pol and Homestead locations are marked by circles. The small square surrounding the Homestead location displays the size of the LES grid.

2. EXPERIMENTAL SETUP

2.1. Observational input data

During IHOP_2002, intensive profiler, radiosonde, and lidar measurements were taken at a field station about 30 km southwest of Beaver, Oklahoma, which was designated as the Homestead site. Three integrated surface flux facility (ISFF) stations were deployed in the Oklahoma and Texas panhandles along an approximately 50 km long, north-south line centered on the Homestead site. Balloon-borne sounding data were available from nearby National Weather Service (NWS) launch sites

at Amarillo, Texas (AMA) and Dodge City, Kansas (DDC). The observational data used for the simulation input also included measurements from the Atmospheric Emitted Radiance Interferometer (AERI) mounted on a 1994 Winnebago (AERIBAGO; Feltz et al. 2003), which was located at the Homestead site. To compare with LES output, CBL depth estimates were available from lidars located at the Homestead site. A map of the study site and input data locations is found in Fig. 1.

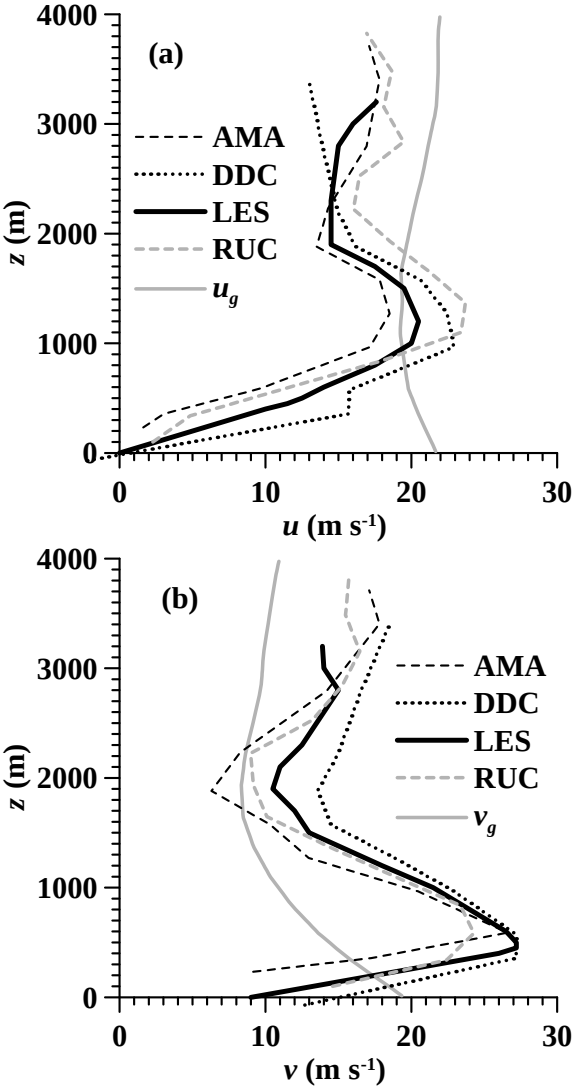

Fig. 2. 1200 UTC wind profiles for the 22 May 2002 case: (a) *x*-component (*u*), and (b) *y*-component (*v*). The solid gray profile is the initial geostrophic wind taken from the nearest RUC analysis grid point.

The initial wind profile data were taken from a combination of the AMA and DDC soundings. Additionally, the large-scale pressure gradient was retrieved from Rapid Update Cycle (RUC) hourly pressure-level analyses, which were obtained from the National Center for Environmental Prediction (NCEP), in order to calculate geostrophic wind vectors. The geostrophic wind was taken to be constant in time during the simulation. The profiles of initial wind and geostrophic wind used in the simulation are shown in Fig. 2 together with wind data from the AMA and DDC soundings.

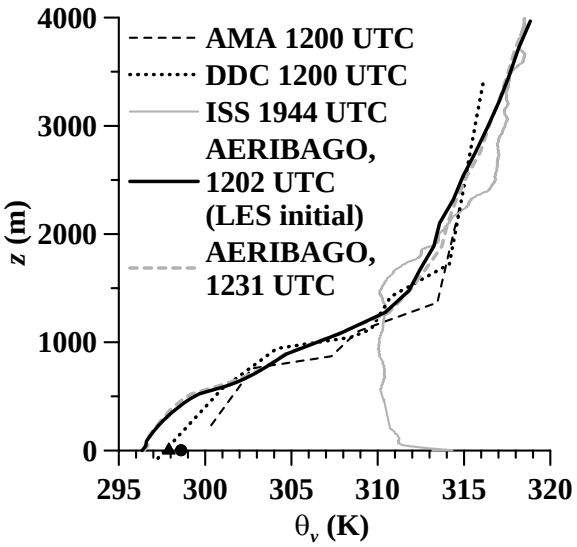

Fig. 1. Virtual potential temperature profiles for the 22 May 2002 CBL case. The black triangle indicates the 3-meter virtual potential temperature at the ISFF2 flux site. The black circle is the ISS virtual potential temperature at the Homestead site.

Table 1. Parameters of Conducted LES

Parameter	**Setting**
Domain size	7.68×7.68×3.99 km^3
Grid	256×256×133 (30-meter cells)
Starting time	1230 UTC
Time step	Evaluated from a numerical stability constraint
Time advancement	Leap-frog scheme with weak Asselin filter
Representation of advection and diffusion terms	Centered second-order finite-difference approximations
Lateral boundary conditions	Periodic for all prognostic variables and pressure
Upper boundary conditions	Neumann with zero gradient for velocity components; a sponge layer imposed in the upper 20% of simulation domain
Lower boundary conditions	No-slip for velocity; Neumann for temperature, pressure and subgrid TKE; Monin-Obukhov similarity functions as in Fedorovich et al. (2001)
Subgrid turbulence closure	Subgrid TKE-based after Deardorff (1980)
Grid frame of reference	u=14 m s^{-1}; v=10 m s^{-1}

The initial LES virtual potential temperature profile was taken from AERIBAGO temperature and water vapor data. The AERI data were compared with AMA and DDC 1200 UTC soundings (see Fig. 3) and found to be reasonably consistent with those data over most of the 4-kilometer depth of the LES domain, except for the lowest few hundred meters. Half-hourly averages of near-surface virtual potential temperature flux from all three ISFF measurement stations were averaged to produce the LES input flux data. The fluxes reached values of approximately 400 W m^{-2} during the middle of the day.

The atmospheric CBL depths were determined from the Holographic Airborne Rotating Lidar Instrument Experiment (HARLIE; Guerra et al. 1999) data. The CBL depth was determined from the lidar data using a Haar wavelet transform as described in Davis et al. (2000). The transform was applied to the one-minute averaged vertical profiles of lidar backscatter (five scans). The same wavelet technique was also applied to the LES potential temperature profiles.

2.2. Numerical setup

The LES code employed in the present study is described in Conzemius and Fedorovich (2006). The LES settings are listed in Table 1. In order to minimize numerical damping of large wavenumber turbulence and to maximize the time step (Conzemius 2004), a moving grid frame of reference was used in the conducted LES runs.

In order to provide a realistic initialization of turbulence, the LES was pre-run for two hours with a weak negative heat flux at the lower surface in order to develop coherent turbulent structures representative of those occurring just after sunrise. The turbulent components of the flow were then saved and added to the initial mean profiles (see Figs. 2 and 3) to provide the initial conditions for the main simulation. Further details of the simulations and observations are provided in Conzemius and Fedorovich (2008).

3. RESULTS OF INITIAL COMPARISON

To take a closer look at the details of the CBL evolution during the simulation, we examine profiles of CBL statistics taken during three times during the simulation. The first is 1252 UTC, when the boundary layer is undergoing transition from a nocturnal planetary boundary layer (PBL) to a sheared CBL. The second is at 1944 UTC, when the CBL evolution is governed primarily by shear-free dynamics. The final time is 0000 UTC (23 MAY), when shear appears to be making a relatively strong contribution to CBL dynamics once again.

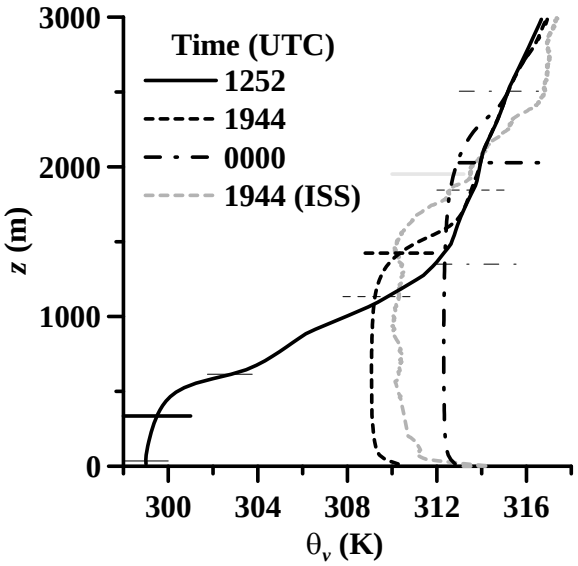

Fig. 4. Mean potential temperature profiles during the simulation of the 22 May 2002 CBL case. See text for notation.

3.1. Evolution of mean profiles

Figs. 4 and 5 show the evolution of the virtual potential temperature and momentum profiles at the indicated times during the case study. The upper and lower limits of the entrainment zone are marked on each profile by thin horizontal lines, and the inversion height zi (identified as the level of maximum entrainment flux within the entrainment zone, retrieved from the buoyancy flux profiles) is shown by bold horizontal lines. The light gray line is the ISS 1944 UTC sounding with the CBL top z_i determined by wavelet transform of the lidar backscatter profile.

At 1252 UTC, the PBL is undergoing transition from nocturnal to CBL, and the entrainment zone encompasses most of the PBL depth because of the strong shear production of turbulence and its dominance over the buoyancy production of TKE (Conzemius and Fedorovich 2008). There is approximately a 15 m s^{-1} velocity increment across the entrainment zone at this time.

At 1944 UTC, the CBL is still growing underneath a rather strong inversion, but the entrainment zone shear has diminished substantially. The layer of very high momentum, seen below z=1500m at 1252 UTC, has largely disappeared due a combination of the entrainment of this momentum into the growing CBL and the effects of the Coriolis and large scale pressure gradient forces (accelerations due to the deviation of the wind from geostrophic balance). The entrainment zone, rather than growing as it typically would under conditions of uniform stratification and shear (see Figs. 10 and 11 of Conzemius and Fedorovich 2006), has not deepened during this time period. By 0000 UTC on 23 May 2002, both the CBL and the entrainment zone become much deeper, influenced by a combination of the weaker

stratification aloft and the increasing shear at the CBL top (13 m s^{-1} compared to 7 m s^{-1} at 1944 UTC).

It is apparent from Fig. 5 that the simulated and observed winds at 1944 UTC are substantially different. Since the pressure gradient changes relatively little during the day of 22 May 2002, the prescription of a constant (in time) geostrophic wind in the LES was assumed to be sufficient. However, the veering of the low-level winds in LES, manifested by an approximately 10 m s^{-1} difference between the simulated and observed *x*-component (*u*) wind at 1944 UTC, is much stronger than it is in the ISS sounding.

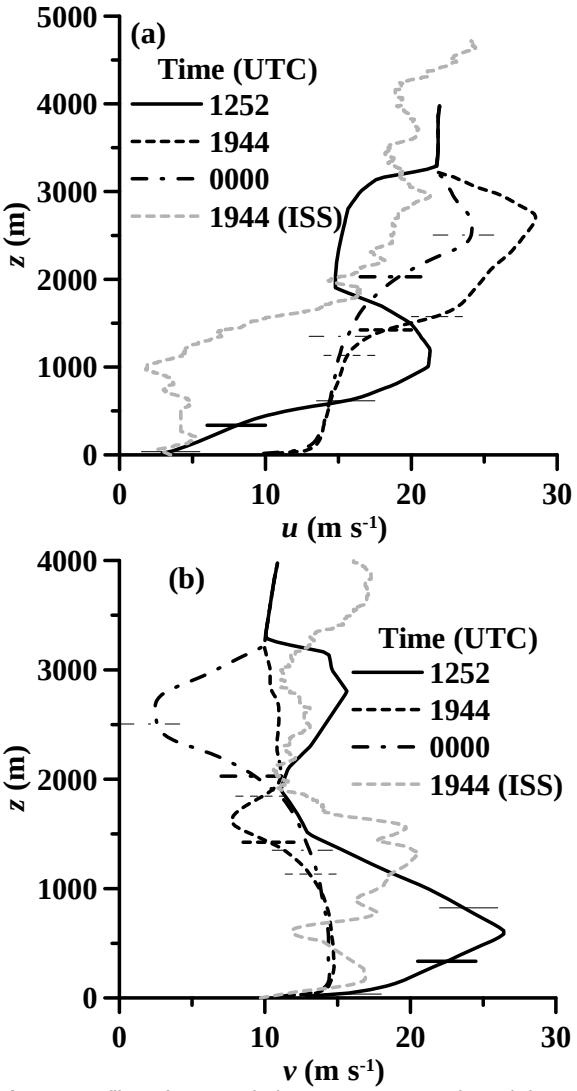

Fig. 5. Profiles of mean wind components at selected times during the simulation of the 22 May 2002 CBL case. See text for notation.

3.2. Simulated CBL depth comparison

The CBL depths determined from HARLIE data are compared with the simulated CBL depth evolution in Fig. 6. The simulated CBL depths agree with the HARLIE CBL depths most closely between 1630 UTC and 1900 UTC. Thereafter, the lidar-determined CBL depths increase rapidly whereas the simulated CBL depth maintains its original rate of growth. Even during the period of relative agreement, the lidar-determined CBL growth rate is somewhat faster than the simulated growth rate, and this difference increases rapidly after 1900 UTC. During the considered interval between 1900 UTC and 2130 UTC, the lidar-determined CBL depth increases nearly 1800 m while the simulated depth increase is about one fourth that amount (just over 400 m).

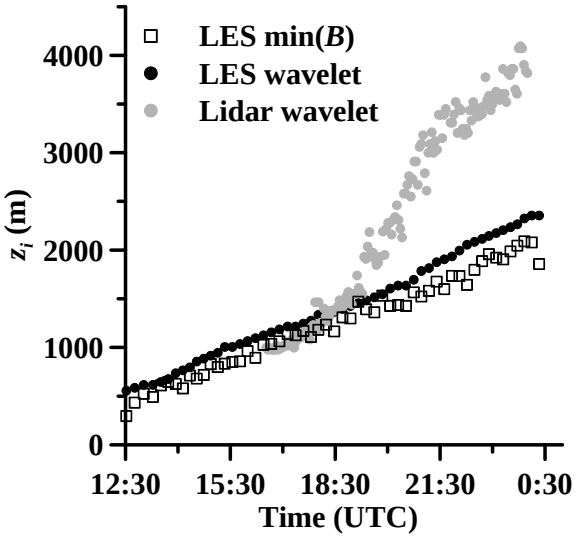

Fig. 6. The CBL depth z_i as a function of time or the 22 May 2002 simulation and concurrent lidar (HARLIE) data.

A look at the 1944 UTC ISS sounding in Fig. 4 reveals that the virtual potential temperature is also larger in the observed mixed layer than in the simulated mixed layer. The difference between AERI potential temperature, which was used for the LES initial conditions, and surface observations is too small to account for the differences in Fig. 4. Rather, the data presented in Weiss et al. (2006) and Demoz et al. (2006) clearly indicate that the dryline, which was located between the Homestead and S-Pol sites in the middle to late afternoon, had a large influence on the CBL structure.

The LES technique is generally not well suited for the type of CBL heterogeneity occurring in this case. In particular, the code does not reproduce the features of the dryline (Demoz et al. 2006; Weiss et al. 2006). The primary difficulty is the necessity of using lateral boundary conditions for CBL scale turbulence. Even if heterogeneous lower boundary conditions such as varying surface fluxes are applied or terrain is added (a general west to east slope as at the study site), the effects of accounting for these types of heterogeneity are eliminated when periodic boundary conditions are applied.

3.3. Simulated versus Observed Turbulence Structure

In Fig. 7, a *y-z* cross section of simulated potential temperature at 1950 UTC is compared to the time-height cross section of signal-to-noise ratio from the FM-CW radar from 1900 UTC to 2000 UTC. In order to make the turbulence structures visually more comparable, the horizontal dimensions of the plots have been adjusted so that the time and space scales displayed correspond to one another. Assuming a mean motion of 20 m s^{-1} in the CBL (from LES data) and using the Taylor frozen turbulence hypothesis to relate spatial and temporal scales of motion, the total time span of one hour in Fig. 7b would correspond to a horizontal domain width of 72 km in Fig. 7a (actual width is 8 km). Likewise, the CBL domain in Fig. 7a corresponds to roughly the first six minutes of Fig. 7b.

Between 1900 and 2000 UTC, the lidar-measured CBL depths were increasing rapidly due to the approach of the dryline. In the FM-CW data, the CBL top is marked by the large gradient in signal-to-noise ratio pointing to the sharp interface between the CBL air and the free atmospheric air. The variability of the interface elevation in FM-CW is significantly larger than it is in LES. The increased variability in the FM-CW data is likely due the effects of greater vertical velocity in the convective plumes as measured by Weiss et al. (2006) in the vicinity of the dryline as well as at the Homestead site (Demoz et al. 2006).

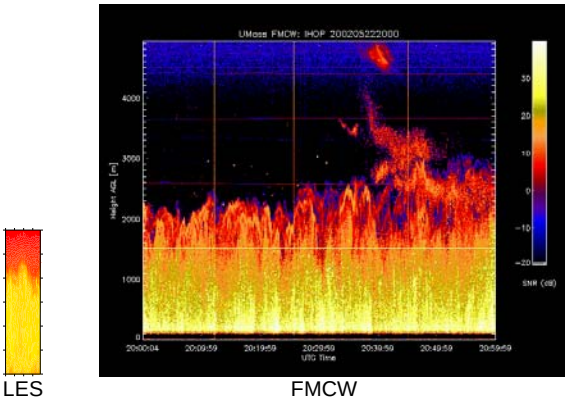

Fig. 7. CBL cross sections at corresponding times during the simulation and observations. See text for explanation.

4. ADDITIONAL SIMULATIONS

Based on the fact that the qualitative synoptic scale pattern did not change much during the course of the day (low pressure remained over the High Plains with a strong northwest to southeast pressure gradient over the Homestead site), the original simulation was performed using a large scale pressure gradient that was constant with respect to time. Also, due to the relatively weak gradients of temperature perpendicular to the prevailing wind direction east of the dryline, the effects of advection were neglected. An analysis of these factors (not shown) revealed that changes in the large scale pressure gradient, indeed, were large enough to explain the discrepancy between the simulations and the observations. Advection, although smaller, was a potentially significant contributor as well.

For these reasons, two additional simulations were conducted. Both simulations relied on RUC analyses as input data to the external forcing terms during the simulation. In the first simulation, the large scale pressure gradients and the advection terms were calculated and updated hour by hour. Since the LES code employs a combined pressure gradient and Coriolis formulation that calculates these forces in terms of the deviation of the flow vector from its geostrophic value, the large scale pressure gradient was used to update the value of the geostrophic wind hour by hour. The advection forces were calculated explicitly from the RUC grid using a centered, second order finite difference.

In the second simulation, the Coriolis and large scale pressure gradients were included in the same manner as in the first. However, rather than compute the advection terms explicitly, a force-restore method was used:

$$\frac{\partial \bar{\phi}(z)_{\mathrm{LES}}}{\partial t} = \frac{\phi(z)_{\mathrm{RUC}} - \bar{\phi}(z)_{\mathrm{LES}}}{t_r} \quad t_r = 3600\mathrm{s}\,.$$

For each variable ϕ, a horizontally averaged vertical profile was calculated. This profile was then compared with the RUC profile of ϕ, and the difference was used as an additional forcing term, which was applied in a constant manner with respect to *x* and *y*, across the entire domain (still a function of *t* and *z*, however) using a restore time scale of t_r.

Results of these simulations showed that the force restore method, overall, worked best to simulate at least the RUC profiles of all CBL scalars. Due to the nonlinear nature of the advection terms, calculating them once per hour from RUC analyses was not frequent enough to sufficiently characterize their behavior during the simulation. Without calculating them from the full 3-D grids as in the larger scale models, using CFL-type conditions, their effects on the flow cannot properly be accounted for in the simulations, and it is best to revert to the simpler force-restore method to bring the LES mean vertical profiles toward closer agreement with RUC analyses.

One must also note that, in this case, with a particularly heterogeneous CBL, that the sharp gradients in CBL depth, potential temperature, and humidity cannot be faithfully represented, even in the RUC analyses, which, in this case, have a 20-km grid interval. Thus, with the force-restore method, the simulated CBL depth does not match that calculated from the vertical profiles of lidar backscatter (Fig. 8) but rather falls approximately halfway in-between the original simulation and the lidar-determined CBL depth. This may be due to the fact that the dryline was located almost exactly over the Homestead site (Demoz et al. 2006), so that the RUC analyses smoothed the gradient in CBL depth, making the RUC-analyzed CBL characteristics over the

Homestead site become a nearly even mix of those on either side of the dryline—cooler, shallower, and more humid to the east of the site and the drier, warmer, and deeper to the west.

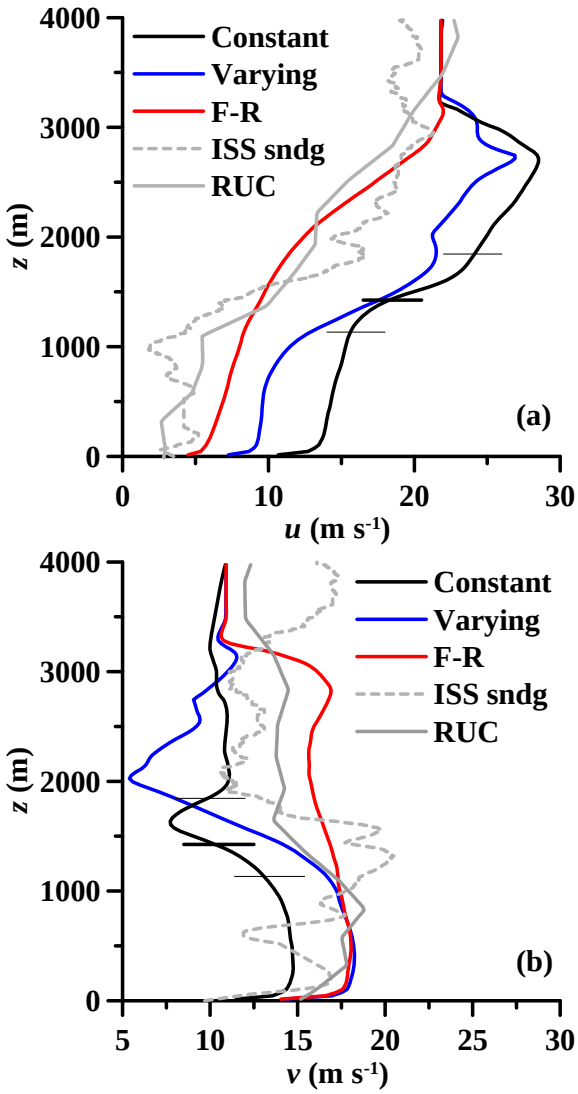

Fig. 8. Comparisons between profiles of velocity components (a) *u* and (b) *v* predicted by the three simulations with large scale pressure gradients constant in time (solid black), varying large scale pressure gradients and advection forces (blue), and using the force-restore method (red). The corresponding ISS sounding (dashed gray) and RUC 2000 UTC analysis (solid gray) are also shown.

The force-restore method seems to provide profiles of wind that most closely match those measured with the ISS sounding (Fig. 9). The simulations with explicitly calculated large scale advection terms did not match the ISS profiles nearly as well. Additionally, just how to formally introduce these larger scale terms into the filtered LES equations of motion remains unknown. Technically, these terms are already larger than the filter scale, so there is an additional separation between the resolved turbulent motions on the grid and the larger-than-domain-scale motions. We have not understood the meaning of the additional terms that result from this third velocity component (larger than domain scale) in the nonlinear term while attempting to derive this new set of LES equations. Although the force-restore method might seem rather crude, it seems to account for all of these unknown terms in a sufficient manner.

The force-restore method also seems not to adversely affect the simulated turbulence structure. Figure 10 shows the horizontal cross-section of virtual potential temperature and velocity from the lowest above-ground level of LES. In all cases, the simulated structure is qualitatively the same. This should be expected, provided the time scale of the force-restore term (an hour) is larger than the convective time scale (typically 20 minutes).

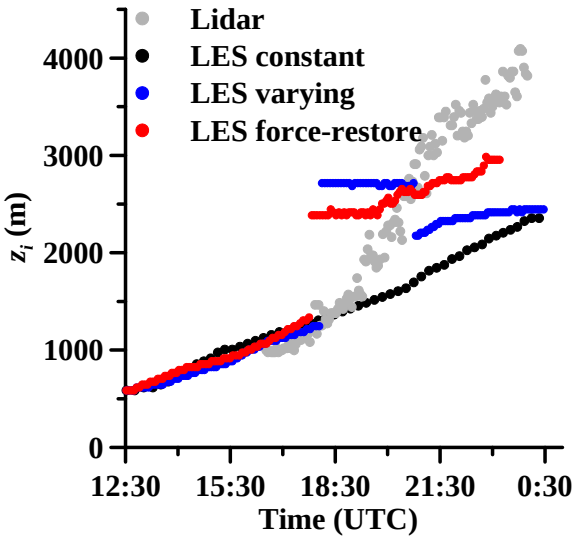

Fig. 9. The CBL depth z_i as a function of time or the three simulations. See Fig. 5 for explanation. The simulation with varying forcing is noted by the blue dots, and the simulation with the force-restore method is indicated with red dots.

5. SUMMARY

The CBL depth increases more slowly with time in the original simulations than in the observations, and the virtual potential temperature profile shows cooler conditions in the mixed layer of the CBL in the simulations. These discrepancies can be explained by the approach of a dryline—the interface between two CBLs of greatly different depths, temperature, and moisture content. Such interfaces are very challenging to simulate due to the constraints imposed by lateral boundary conditions, which are usually chosen as periodic. Meanwhile, disagreements between simulated and observed velocity profiles are probably more easily resolved by accounting for the time variation of the large scale pressure gradients, as well as the advection of temperature and velocity components, in LES.

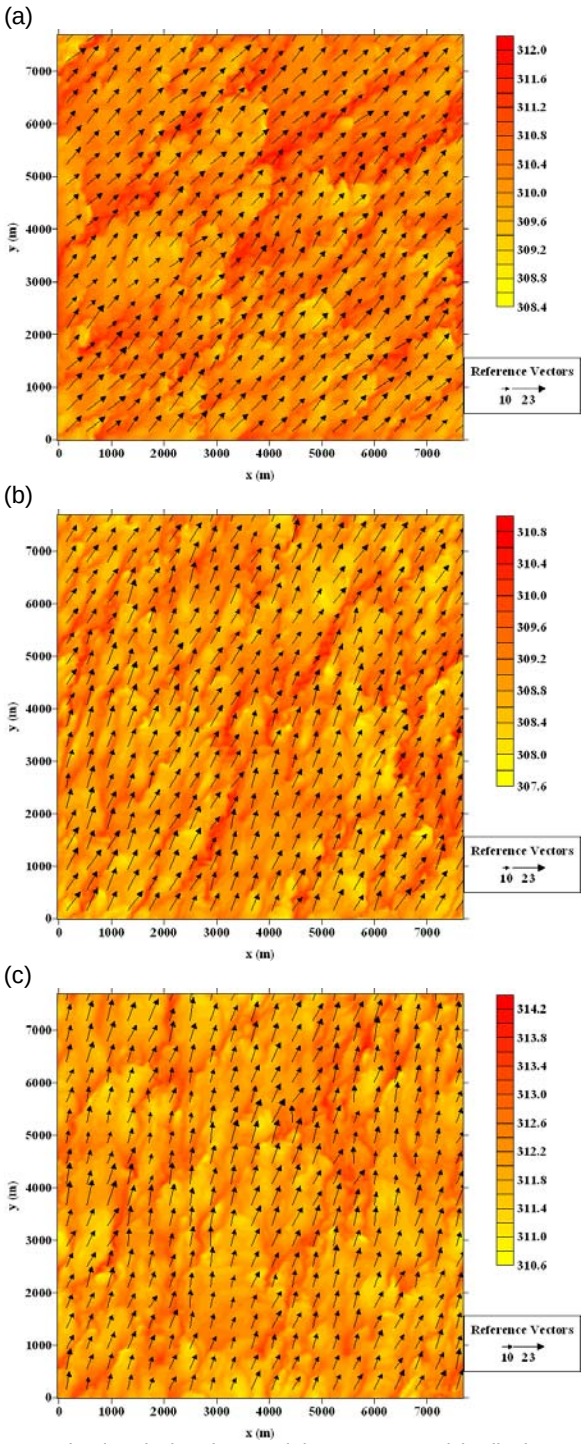

Fig. 10. Simulated virtual potential temperature (shading) and wind vectors for all three simulations: (a) constant forcing; (b) varying forcing; and (c) force-restore.

New simulations with advection and the time variation of large scale pressure gradients included did not show an appreciable improvement in the ability of the simulation to reproduce the evolution of the observed CBL on 22 MAY 2002. This may be mostly due to the insufficiently frequent update of the advection terms calculated from hourly analyses. The prescription of the larger scale terms within the LES equations of motion are also difficult to formalize. The meanings of the additional terms that result are unclear.

Rather, the best method to reproduce the observed CBL evolution is to use a force-restore term, applied to the LES horizontally averaged profiles, to bring the mean profiles back to the RUC hourly analyses on a time scale that is larger than the convective time scale for the CBL.

ACKNOWLEDGEMENTS.

The research presented here was supported by National Science Foundation grant ATM-0124068. The first author would like to thank members of his Ph.D. advisory committee Charles A. Doswell III, Brian Fiedler, Randall Kolar, Douglas Lilly, and Alan Shapiro for their motivation to conduct the initial simulation in this study.

REFERENCES

Conzemius, R. J., 2004: The effects of wind shear on the convective boundary layer entrainment. Ph.D. dissertation, University of Oklahoma, 338 pp.

Conzemius, R. J., and E. Fedorovich, 2006: Dynamics of sheared convective boundary layer entrainment. Part I: methodological background and large eddy simulations. *J. Atmos. Sci.,* **63,** 1151-1178.

Conzemius, R. J., and E. Fedorovich, 2008: A case study of convective boundary layer development during IHOP_2002: numerical simulations compared to observations. *Mon. Wea. Rev.,* in press.

Davis, K. J., N. Gamage, C. R. Hagelberg, C. Kiemle, D. H. Lenschow, and P. P. Sullivan, 2000: An objective method for deriving atmospheric structure from airborne lidar observations. *J. Atmos. Oceanic Technol.,* **17,** 1455–1468.

Deardorff, J. W., 1980: Stratocumulus-capped mixed layers derived from a three-dimensional model. *Bound.-Layer Meteor.*, **18**, 495-527.

Demoz, B., and Coauthors, 2006, The dryline on 22 May 2002 during IHOP_2002: convective-scale measurements at the profiling site. *Mon. Wea. Rev.,* **134,** 294-310.

Fedorovich, E., F. T. M. Nieuwstadt, and R. Kaiser, 2001: Numerical and laboratory study of horizontally evolving convective boundary layer. Part I: Transition regimes and development of the mixed layer. *J. Atmos. Sci.*, **58**, 70-86.

Feltz, W. F., H. B. Howell, R. O. Knuteson, H. M. Woolf, and H E. Revercomb, 2003: Near continuous profiling of temperature, moisture, and atmospheric stability using the atmospheric

emitted radiance interferometer (AERI). *J. Appl. Meteor.,* **42,** 584-597.

Guerra, D., G. Schwemmer, A. Wooten, S. Chaudhuri, T. Wilkerson, 1999: Prototype holographic atmospheric scanner for environmental remote sensing. *J. Geophys. Res.*, **104**, (D) 22,287-22,292.

Moeng, C.-H., J. Dudhia, J. Klemp, and P. P. Sullivan, 2007: Examining two-way grid nesting for large eddy simulation of the PBL using the WRF model. *Mon. Wea. Rev.,* **135**, 2295-2311.

Moeng, C.-H., and P. P. Sullivan, 1994: A comparison of shear- and buoyancy-driven planetary boundary layer flows. *J. Atmos. Sci.,* **51,** 999-1022.

Pino, D., J. V.-G. de Arellano, and P. J. Duynkerke, 2003: The contribution of shear to the evolution of a convective boundary layer. *J. Atmos. Sci.,* **60,** 1913-1926.

Weckwerth, and Coauthors, 2004: An overview of the International H_2O Project (IHOP_2002) and some preliminary highlights. *Bull. Amer. Meteor. Soc.,* **85,** 253–277.

Weiss, C., H. B. Bluestein, and A. L. Pazmany, 2006: Finescale radar observations of the 22 May 2002 dryline during the International H_2O Project (IHOP). *Mon. Wea. Rev.,* **134,** 273-293.